

Cite this article as: Meng Linggang, Wu Xiaohui, Xing Qingyuan, et al. Effect of Element Cu on Microstructure Evolution and Corrosion Resistance of Al-Zn-Mg-Er-Sc-Zr Alloy[J]. Rare Metal Materials and Engineering, 2022, 51(12): 4475-4482.

ARTICLE

Effect of Element Cu on Microstructure Evolution and Corrosion Resistance of Al-Zn-Mg-Er-Sc-Zr Alloy

Meng Linggang¹, Wu Xiaohui¹, Xing Qingyuan², Ya Bin¹, Zhou Bingwen¹, Zhu Xiurong³, Zhang Xingguo¹

¹School of Materials Science and Engineering, Dalian University of Technology, Dalian 116024, China; ²AEECC Beijing Institute of Aeronautical Materials, Beijing 100095, China; ³Ningbo Branch, Ordnance Science Institute of China, Ningbo 315103, China

Abstract: The formation and evolution of the $\text{Al}_8\text{Cu}_4\text{Er}$ phase and its influence on the corrosion resistance of Al-Zn-Mg-Er-Sc-Zr alloys were studied by changing the element content of Cu. The results show that with the increase in Cu content, the grains of the alloy are significantly refined, but at the same time, different types of residual phases in the solid-solution-state of the alloy increase. There is a companion relationship between the $\text{Al}_8\text{Cu}_4\text{Er}$ phase and the Al-Fe phase, and they achieve phase transformation through the interaction between Cu and Fe. It can be expressed as the relationship: $\text{Al}_6\text{Fe} \xrightarrow{\text{Cu}} \text{Al}_{60}\text{Cu}_{30}\text{Fe}_{10} \xrightarrow{\text{Er}} \text{Al}_8\text{Cu}_4\text{Er}$. The intergranular corrosion of alloys with different compositions shows pitting characteristics closely related to the residual phase. Although the Al-Fe phase containing Cu and Er has a smaller corrosion pit size, the network distribution characteristics increase the corrosion depth, while the $\text{Al}_8\text{Cu}_4\text{Er}$ with better corrosion resistance has a serious decline in the counterpart of the alloy due to its tendency to coarsen and interactive relationship with the Al-Fe phase.

Key words: Al-Zn-Mg-Cu-Er alloy; $\text{Al}_8\text{Cu}_4\text{Er}$ phase; Al-Fe phase; corrosion properties

The 7xxx series aluminum alloys have been extensively used in the aerospace field for their high strength, high modulus and low density. However, they show unsatisfying corrosion resistance, thus restricting their safety in use^[1-3]. Adding trace rare earth elements and transition elements can refine grains significantly and improve dendritic segregation, which can improve corrosion resistance of alloys^[4-6]. Specifically, Sc is the most effective. The addition of Sc can form a dispersed phase Al_3Sc coherent with the matrix. Al_3Sc has a fine grain strengthening effect and substructural reinforcement effect, thus improving the comprehensive mechanical properties of alloys^[7,8]. However, Sc is very expensive, making it unpracticable to be applied extensively in industrial production.

The price of Er is relatively lower than that of Sc. The products of Al_3Er and Al_3Sc are both L_{12} -type compounds. Er is viewed as the ideal substitute for Sc since it has a similar effect^[9,10]. Adding Er into the 7xxx series aluminum alloys can

form primary and secondary Al_3Er particles. Not only can they refine the as-cast grains, but also stabilize sub-structure and inhibit recrystallization effectively and have ideal refining and strengthening effects on alloys^[11,12]. When Cu is added into the aluminum alloys, the existence form and effect of Er may change significantly. Large-sized $\text{Al}_8\text{Cu}_4\text{Er}$ phase is generated after the reaction of Er and Cu, which is difficult to be dissolved in the matrix. Some researchers^[13,14] believed that the $\text{Al}_8\text{Cu}_4\text{Er}$ phase is easy to be crushed during the deformation of alloys, thus initiating cracks. This is undesirable for the comprehensive performances of alloys. Some researchers^[15] also pointed out that the $\text{Al}_8\text{Cu}_4\text{Er}$ phase can change the continuous distribution of the S-phase at grain boundaries into a discontinuous pattern, which can improve the resistance to intergranular corrosion of alloy.

At present, there is no agreement on the generation mechanism and influencing mechanism of the $\text{Al}_8\text{Cu}_4\text{Er}$ phase. Besides, studies on the $\text{Al}_8\text{Cu}_4\text{Er}$ phase are carried out under

Received date: January 25, 2022

Foundation item: National Key Research and Development Program of China (2018YFA0702900); Science and Technology Innovation Major Project of Ningbo (2019B10101)

Corresponding author: Meng Linggang, Ph. D., Associate Professor, School of Materials Science and Engineering, Dalian University of Technology, Dalian 116024, P. R. China, E-mail: menglg@dut.edu.cn

Copyright © 2022, Northwest Institute for Nonferrous Metal Research. Published by Science Press. All rights reserved.

the changes of Er content. However, the influences of Cu on phase formation are hardly reported yet. In this study, influences of formation and evolution of the Al_8Cu_4Er phase on corrosion performances of alloys were investigated by analyzing structural evolution, corrosion potential and corrosion current density of Al-Zn-Mg-Er-Sc-Zr alloys with different Cu contents.

1 Experiment

In this experiment, three self-made high-strength aluminum alloys with different Cu contents were prepared by the iron mold casting method. The raw materials for smelting alloys were pure Al (99.9wt%), Zn (99.9wt%), Mg (99.9wt%) and master alloys of Al-50Cu, Al-20Er, Al-2Sc, Al-5Zr Alloy, and the chemical compositions are shown in Table 1.

The well resistance furnace (SG-5-10) was used for smelting, while an iron mold and graphite crucible were also used in the process. During the smelting process, the stirring, refining and pouring temperatures were kept between 720 and 740 °C. The ingot was then subjected to two-stage solution treatment. The specific process was as follows: the first stage solution treatment at 400 °C for 4 h, and the second stage solution treatment at 470 °C for 48 h. During the heating process, the heating rate was maintained at about 3 °C/min, and when the furnace temperature reached 465 °C, the heating rate was adjusted to 1 °C/min; the temperature was slowly raised to prevent the samples from over-burning, and finally they were subjected to water-cooled quenching to room temperature.

The intergranular corrosion (IGC) test was carried out according to the GB/T 7998-2005 standard. The solid solution alloy was cut into a 10 mm×10 mm×20 mm sample and immersed in NaCl-H₂O₂ solution for 6 h. The solution temperature was kept at 35±2 °C. After grinding and polishing, the maximum corrosion depth of the sample was observed by the optical microscope. Electrochemical tests were performed in 3.5% NaCl solution at room temperature using a three-electrode system. The polarization scanning range of polarization curve test was ±0.3 V (vs OCP), and the scanning rate was 1 mV/s; the alloy sample was served as the working electrode, the calomel electrode was the reference electrode, and the platinum electrode was the auxiliary electrode. After the open-circuit potential was stable, the polarization curve of the alloy was measured. To ensure the accuracy of the results, three data groups were measured and averaged. The immersion corrosion test solution was also 3.5% NaCl solution, and the solution temperature was kept at 25±2 °C. It was ensured that the experimental surface was parallel to the solution during the experiment. After soaking

the samples for 6 h and washing them in clean water, the mixture solution of 50 mL of phosphoric acid, 20 g of chromium trioxide and 1000 mL of deionized water was used to clean the corrosion products by ultrasonic vibration, and finally the surface corrosion morphology was observed by the electron probe. The in-situ corrosion test solution also selected 3.5% NaCl solution. After grinding and polishing the solid solution sample, the samples were placed in the solution and taken out at different intervals to observe the change of the selected grain boundary phases.

The actual chemical compositions of the alloys were detected by an XRF-1800 X-ray fluorescence spectrometer (Shimadzu, Japan). Optical microscopy (OM, LEICA DMi8), transmission electron microscopy (TEM, JEM F200), laser scanning confocal microscope (LSCM, OLS4000) and electron probe microscopy (EPMA, JXA-8530F Plus) were employed to characterize the microstructure. The second phase composition and element distribution were analyzed by wavelength dispersive spectrum (WDS). The polarization curves of the alloys were measured by a Gamry reference 600 electrochemical workstation, and the corrosion potential and corrosion current density were calculated by fitting analysis. Image-pro software was used for analysis of statistics and images.

2 Results and Discussion

2.1 As-cast and solid-solution-state microstructural characteristics of alloy

The as-cast metallographic structure and solid-solution backscattered electron (BSE) images of alloys with different Cu contents are shown in Fig. 1. According to the comparison of as-cast structures, adding Cu has a relatively obvious refining effect on the as-cast structures. In particular, grain size decreases significantly after adding 1wt% Cu. The average grain size decreases from 317 μm of Cu-free sample to 164 μm. Adding Cu can increase the residual phases at crystal boundaries after the solid dissolution of alloy. When the Cu content increases from 0.5wt% to 1wt%, the crystal boundary phase distribution changes from continuous to discontinuous. In the consolidation process of alloys, adding Cu can facilitate the formation of the secondary phases in front of the solid-liquid interface along the crystal boundaries. These phases can hinder grain growth to some extent, thus refining grains. However, Cu-containing phases generally have a high melting point and they are extremely easy to produce abundant residues at crystal boundaries after the solid dissolution^[16].

2.2 Evolution characteristics of secondary phases at grain boundary

Representative three alloys were chosen for local element surface scanning analysis to determine the composition and structural characteristics of insoluble phases in solid-solution alloys. The surface scanning distribution of major elements are shown in Fig. 2, and the corresponding chemical composition analysis results are shown in Table 2.

Gray Al-Fe phase (Position 1) and attached bright white

Table 1 Chemical compositions of the experimental alloys (wt%)

Alloy	Zn	Mg	Cu	Er	Sc	Zr	Fe	Al
1#	9.08	1.85	-	0.09	0.13	0.10	0.12	Bal.
2#	9.12	1.77	0.49	0.11	0.12	0.11	0.12	Bal.
3#	8.92	1.77	1.04	0.11	0.10	0.11	0.13	Bal.

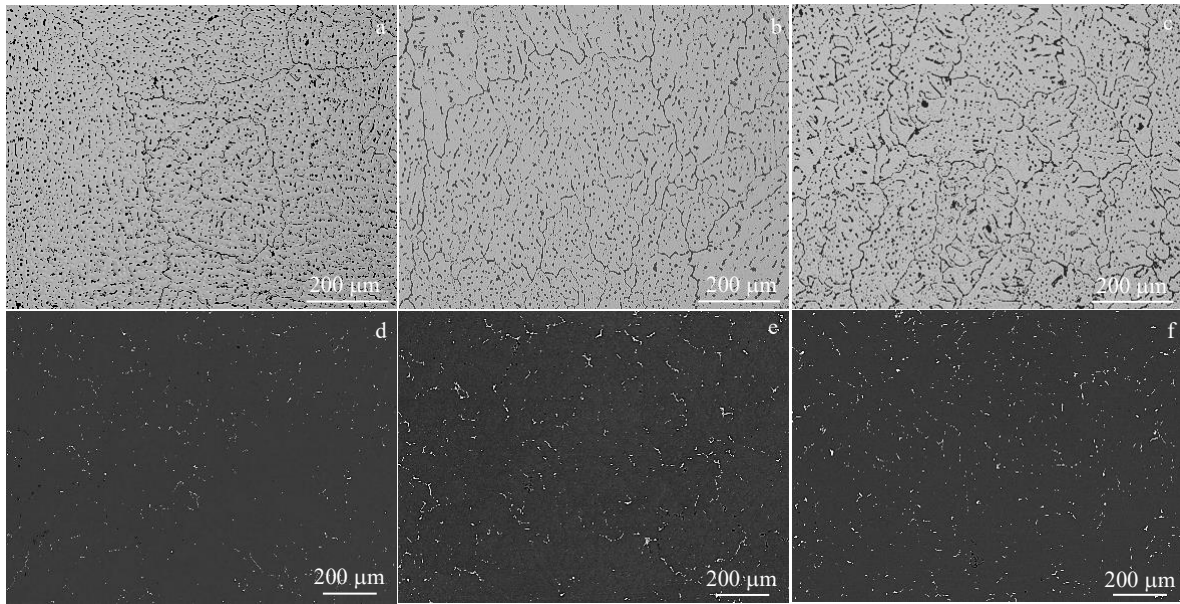


Fig.1 OM microstructures of as-cast (a, b, c) and BSE images of the solid solution (d, e, f) alloys: (a, d) Cu-free, (b, e) 0.5wt% Cu, and (c, f) 1wt% Cu

Al_3Er phase (Position 2) become a dominant role in the Cu-free sample. When Cu content is 0.5wt%, insoluble phases in alloy do not change significantly. Some Er and Sc also attach around the Al-Fe phase in the form of flocculent Al-Er-Sc ($\text{Al}_3(\text{Er}, \text{Sc})$) phase, but grain size increases significantly. The rest of Er covers the Al-Fe phase to form a bright white Al-Er-Fe phase (Position 4). According to white circles in Fig.2h and 2i, there are significant interactions between Er and Fe. Under this circumstance, Cu dissolves in the gray Al-Fe phase (Position 5) without Er or with low Er content. Moreover, there is no significant association between Er and Cu. When Cu content reaches 1wt%, the bright white insoluble phases

are typical $\text{Al}_8\text{Cu}_4\text{Er}$. Some remains still attach to the Al-Fe phase (Position 6) and contain a high Sc content. The rest phases grow independently (Position 7). In this case, Sc content drops sharply.

Element surface scanning distributions are shown in Fig.2. It can be seen from Fig.2g and 2h that Cu is extremely easy to dissolve in Fe-containing phases and matrix. It is only separated when the $\text{Al}_8\text{Cu}_4\text{Er}$ phase is produced, as shown in Fig.2l and 2m. In Fig.2c, 2d, 2e, 2h, 2i and 2j, there are some associations among Er, Sc and Fe. Such associations are ended only when the $\text{Al}_8\text{Cu}_4\text{Er}$ phase is generated.

In the 2# alloy with a low Cu content, there are significant

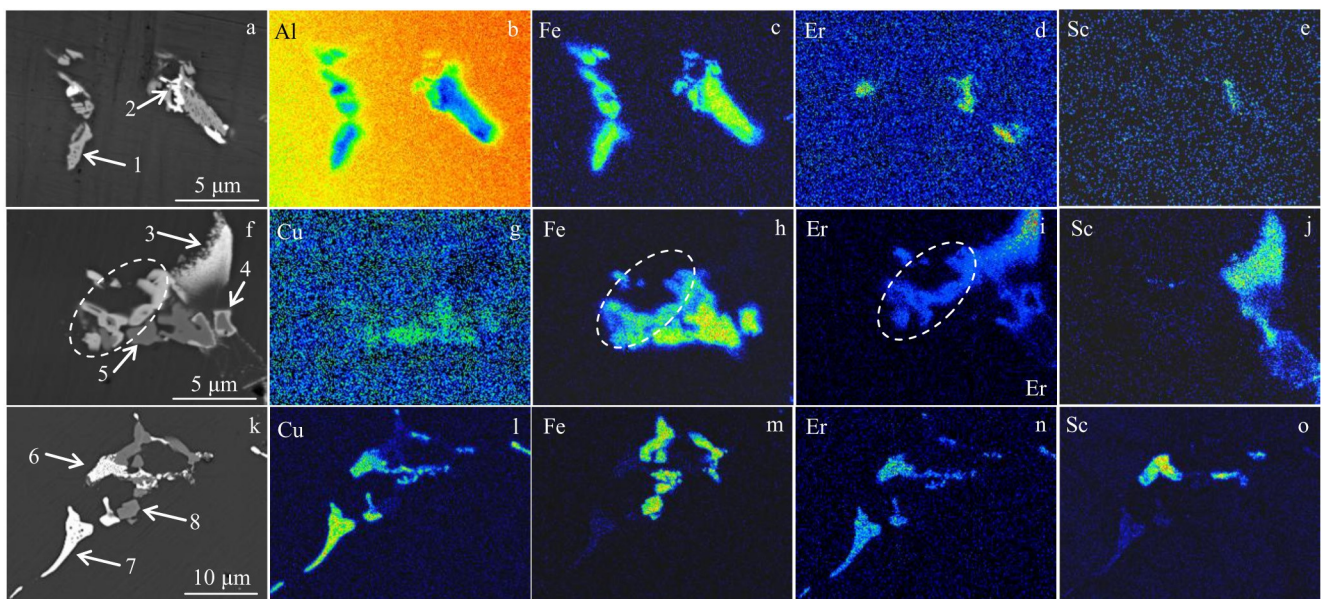


Fig.2 BSE images of the solid solution alloys (a, f, k) and corresponding element distributions of Al (b), Cu (g, l), Fe (c, h, m), Er (d, i, n), and Sc (e, j, o): (a~e) Cu-free, (f~j) 0.5wt% Cu, and (k~o) 1wt% Cu

Table 2 Chemical compositions of points marked in Fig.2 (at%)

Point	Al	Zn	Mg	Cu	Er	Sc	Fe
1	82.15	1.40	0.84	-	0.34	0.17	15.36
2	73.62	2.35	0.45	-	17.79	5.13	0.22
3	79.38	1.73	0.99	0.14	6.73	9.52	1.01
4	80.46	0.77	0.76	0.55	5.94	0.12	11.35
5	77.46	1.81	0.94	2.28	0.12	0.18	17.24
6	54.93	8.77	1.19	22.14	5.85	6.75	0.45
7	57.78	8.55	1.05	26.15	5.40	0.54	0.51
8	80.80	2.52	0.13	2.83	0.01	0.01	13.67

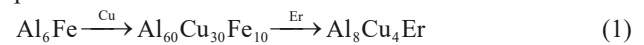
interactions between Er and Cu as well as between Fe and Cu, such as the bright white Al-Fe phase containing Er at Position 4 and the gray Al-Fe phase containing Cu at Position 5. However, Er and Cu are bonded significantly rather than separated in the 3# alloy with higher Cu content. At this moment, Er and Cu are both separated from Fe. The $\text{Al}_8\text{Cu}_4\text{Er}$ phase, formed by bonding of Er and Cu, is closely related to the Al-Fe phase, showing associations.

To verify such association, a hybrid phase in the 3# alloy is chosen and thin films are collected by dual focused ion beams for transmission electron microscope analysis (Fig.3).

It can be determined through analysis of diffraction spots that the bright phases in the backscattering images are $\text{Al}_8\text{Cu}_4\text{Er}$ phase and the dark phases are Al-Fe phase. However, they are not a single-phase but a cluster of many Fe-containing phases (Fig.3b). The large-scaled phases with dark contrast are $\text{Al}_{60}\text{Cu}_{30}\text{Fe}_{10}$, accompanied by some small round particle phases, which are Al_6Fe . The strong interaction between Cu and Fe forms the $\text{Al}_{60}\text{Cu}_{30}\text{Fe}_{10}$ phase, while interaction between Cu and Er forms the $\text{Al}_8\text{Cu}_4\text{Er}$ phase. Clearly, Cu is the bridge between the two phases. In the solid

solution treatment, Cu and Er at other positions are dissolved normally in the matrix. Only Cu and Er near the Fe-containing phases interact with Fe. The formation and growth of the $\text{Al}_8\text{Cu}_4\text{Er}$ phase require the $\text{Al}_{60}\text{Cu}_{30}\text{Fe}_{10}$ phase as the attachment. With the continuous growth of the $\text{Al}_8\text{Cu}_4\text{Er}$ phase, it is separated from the Al-Fe phase gradually and becomes increasingly independent, as shown in Position 7 in Fig.2k.

To sum up, the $\text{Al}_8\text{Cu}_4\text{Er}$ phase forms after solid solution, which mainly relies on the formation and growth of Al-Fe phases. There are associations between the $\text{Al}_8\text{Cu}_4\text{Er}$ phase and the Al-Fe phase. $\text{Al}_{60}\text{Cu}_{30}\text{Fe}_{10}$ serves as the key connector between them. Due to interaction between Cu and Fe, Al_6Fe is transformed into $\text{Al}_{60}\text{Cu}_{30}\text{Fe}_{10}$. $\text{Al}_{60}\text{Cu}_{30}\text{Fe}_{10}$ further interacts with Er to form the $\text{Al}_8\text{Cu}_4\text{Er}$ phase. With changes of Cu and Er contents, the $\text{Al}_8\text{Cu}_4\text{Er}$ phase grows gradually until it is separated from the associated phases. This process is expressed as follows:



According to the characteristics of Al-Er-Fe at Position 4 in Fig. 2, it can be judged preliminarily that Er, which is dissolved in the Al-Fe phase, is one of the key factors assuring the reaction. The specific effect mechanism of Er has to be further analyzed and determined.

2.3 Corrosion resistance

Intergranular corrosion morphologies of solid-solution alloys with different Cu contents are shown in Fig.4. Adding Cu can influence the corrosion performance of the alloy significantly. All three alloys present pitting corrosion morphologies. With the increase in Cu content, insoluble phases at crystal boundary increase and the corrosion is intensified. The depth and width of the largest corrosion pit increase significantly.

Polarization curves of solid-solution alloy obtained through

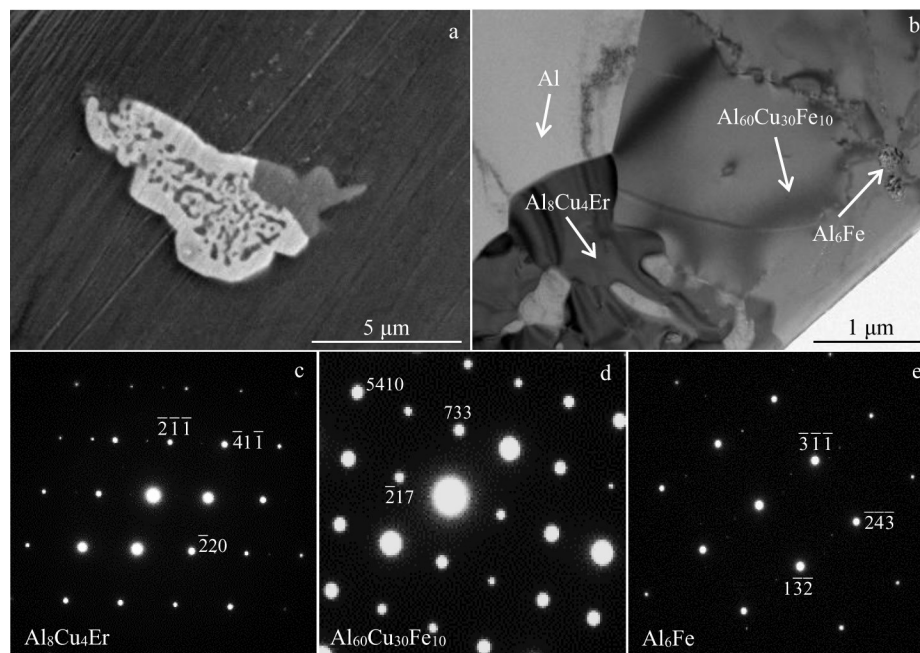


Fig.3 BSE image (a) and TEM image (b) of insoluble phases of solid-solution 3# alloy and corresponding SAED patterns (c-e)

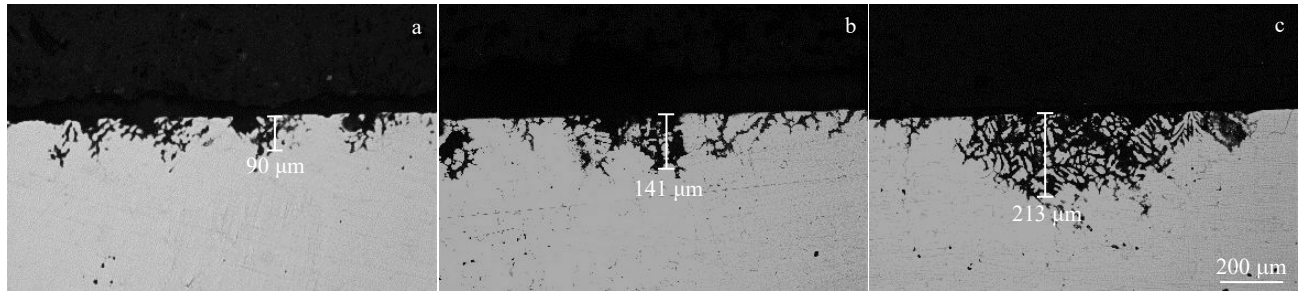


Fig.4 IGC morphologies of solid-solution alloys with different Cu contents: (a) Cu-free, (b) 0.5wt% Cu, and (c) 1wt% Cu

the electrochemical test are shown in Fig. 5. Corrosion potentials and corrosion current density, which are fitted by polarization curves, are listed in Table 3. Obviously, the corrosion potential of alloys increases gradually after Cu is added. Corrosion potential is a thermodynamic parameter, and it reflects the corrosion tendency of alloys in the serving environment. Corrosion potential is negatively related to the corrosion tendency of alloys. Adding Cu weakens the corrosion tendency of alloys. However, adding Cu may increase the corrosion current density of alloys. Corrosion current density is a kinetic parameter and it actually reflects the corrosion rate of alloys in the corrosion environment. Corrosion current density is positively related to the corrosion rate of alloy. Results demonstrate that with the increase in Cu content, the corrosion rate of the alloy increases, and corrosion resistance decreases. This is closely related to residues and the distribution of crystal boundary phases.

To compare the pitting corrosion resistance of alloys with different Cu contents, three alloys were immersed in 3.5% NaCl solution for 6 h. Later, they were taken out and

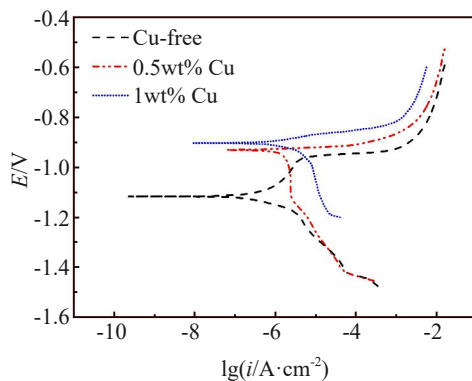


Fig.5 Polarization curves of the solid-solution alloys density

Table 3 E_{corr} and i_{corr} of the solid-solution alloys obtained from the polarization curves

Alloy	Corrosion potential, E_{corr}/V	Corrosion current density, $i_{\text{corr}}/\times 10^{-6} A \cdot \text{cm}^{-2}$
1#	-1.117	0.729
2#	-0.923	1.52
3#	-0.880	5.70

corrosion products were eliminated. The surface corrosion morphologies are shown in Fig. 6. Fig. 6a~6c are secondary electron images of the corrosion surfaces of the three alloys. The left upper corner is the high-magnification image of the representative position. Fig. 6d~6f are laser confocal images of corrosion surfaces of them. S_a is the surface roughness. The higher value of S_a indicates a higher degree of corrosion. It can be seen from Fig. 6a that the 1# alloy without Cu has a relatively regular corrosion surface and the corrosion pits are basically consistent in size. Moreover, secondary phases almost have been fallen off in 2# alloy with 0.5wt% Cu content, and the number of corrosion pits increases. It can also be seen from Fig. 6b that there are phase residues in most of the corrosion pits. Large corrosion pits are developed in the 3# alloy with 1wt% Cu. It also can be seen from Fig. 6c that there are a few residual phases in corrosion pits.

After analyzing the composition of the residual phases of 2# and 3# alloys, the relevant results are shown in Fig. 7 and Table 4. Among them, the residual phases of 2# alloys are continuous bone-like, as shown in Fig. 7a~7c, and in the 3# alloys, the residual phases are fragmented, as shown in Fig. 7d~7f. No obvious residual phases are found in 1# alloy. Combined with the previous microstructure analysis, it can be seen that the insoluble phases in 1# alloy are mainly the Al-Fe phase and the Al_3Er phase attached. The potential of the Al_3Er phase is lower than that of the matrix, and the corrosion process will corrode first as the anode. The potential of Al-Fe is higher than that of the matrix. It serves as the cathode during corrosion, while the surrounding matrix serves as the anode to accelerate corrosion of the matrix. Finally, some small-sized insoluble phases fall off during ultrasonic cleaning in alloys^[17]. Residual phases in corrosion pits in the 2# alloys are mainly attributed to the Al-Fe phase, which has the solid solution of Cu or Er (Fig. 7a~7c). Under this circumstance, the Al-Fe phase exhibits a continuous skeleton morphology, and some phases have a large number of pores (Fig. 7c). The continuous growth of phases is corresponding to solid-solution structure in Fig. 1e. This is also the major reason why the corrosion depth of 2# alloy is higher than that of 1# alloy. The development of such morphological phases is closely related to the interactions of Er and Cu with Fe. According to phase composition in Fig. 7c, this phase is the Al-Fe phase which has solid dissolution of Er. Combined with structural characteristics of the Al-Fe phase at Position 4 in Fig. 2f, the

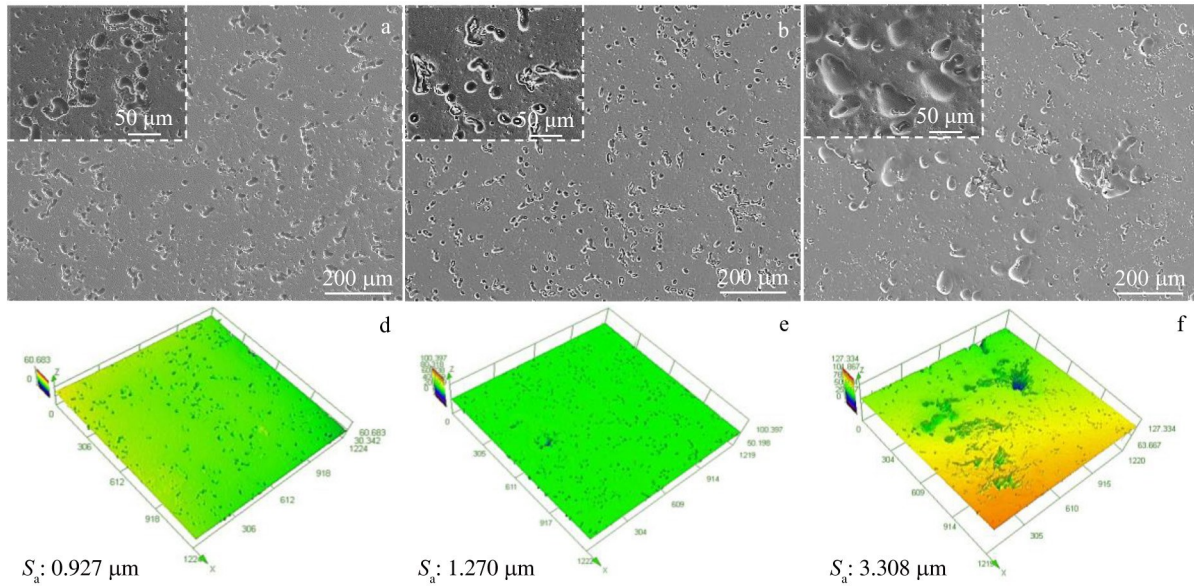


Fig.6 SE images (a, b, c) and three-dimensional corrosion morphologies (d, e, f) of solid solution alloys after immersion corrosion: (a, d) Cu-free, (b, e) 0.5wt% Cu, and (c, f) 1wt% Cu

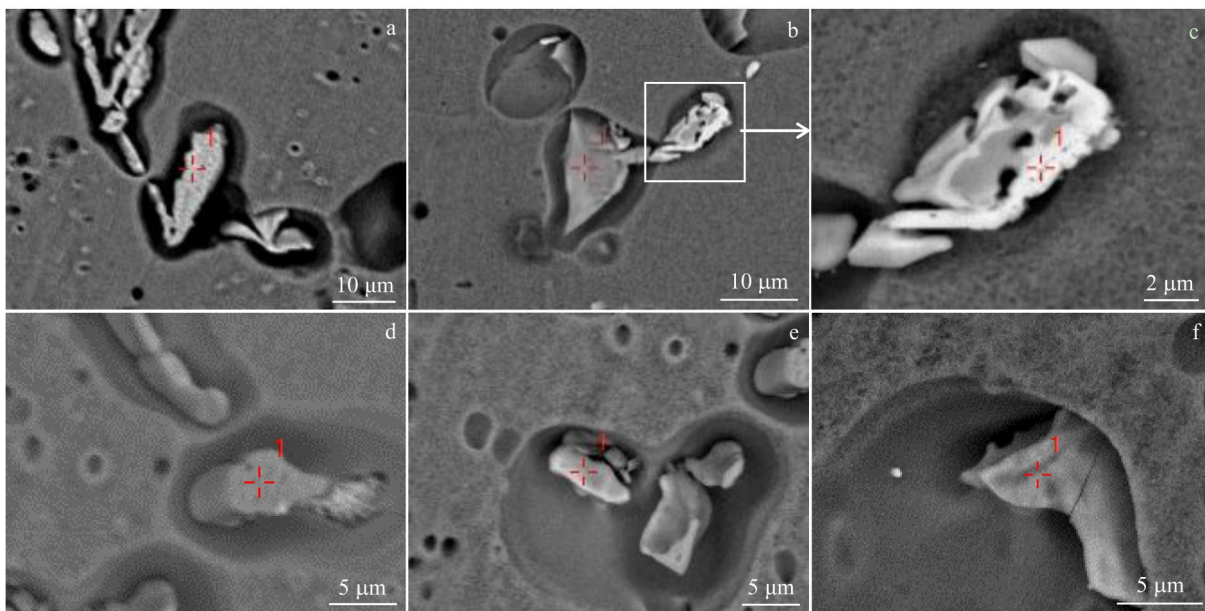


Fig.7 Residual phases of alloy 2# (a~c) and 3# (d~f) after immersion corrosion: (a, b, d, e, f) Al-Fe-(Cu) and (c) Al-Fe-(Er)

unique pore characteristics of the Al-Fe phase is associated with the formation and transition of these pores. This is also the prerequisite for the associated growth of the Al_8Cu_4Er and Al-Fe phase under high Cu content. Al_8Cu_4Er phase is not discovered in residual phases of 3# alloy, and only the bulk Al-Fe phase is found. Hence, large corrosion pits in alloys are caused by the large-sized Al_8Cu_4Er phase. Some Al_8Cu_4Er phases are attached to the Al-Fe phase. They act as cathodes during the corrosion process, accelerating the corrosion of the surrounding Al matrix and falling off during ultrasonic cleaning, leaving only some Al-Fe phase.

To compare corrosion degree between the Al_8Cu_4Er phase and Al-Fe phase, in-situ corrosion of grain boundary phases in

Table 4 Chemical compositions of points marked in Fig.7 (at%)

Fig.	Al	Zn	Mg	Cu	Er	Sc	Fe
7a	83.75	2.51	0.82	2.13	0.03	0.04	10.67
7b	81.56	2.73	2.19	2.16	0.02	0.02	11.16
7c	81.51	2.28	0.91	0.62	2.86	0.96	10.42
7d	80.74	2.50	0.13	2.57	0.02	0.36	13.65
7e	79.46	1.85	1.38	2.73	0.02	0.11	14.19
7f	80.75	2.22	1.59	2.65	0.03	0.07	12.49

the 3# alloy was observed. Results are shown in Fig.8.

It can be seen from Fig. 8a and 8b that the corrosion

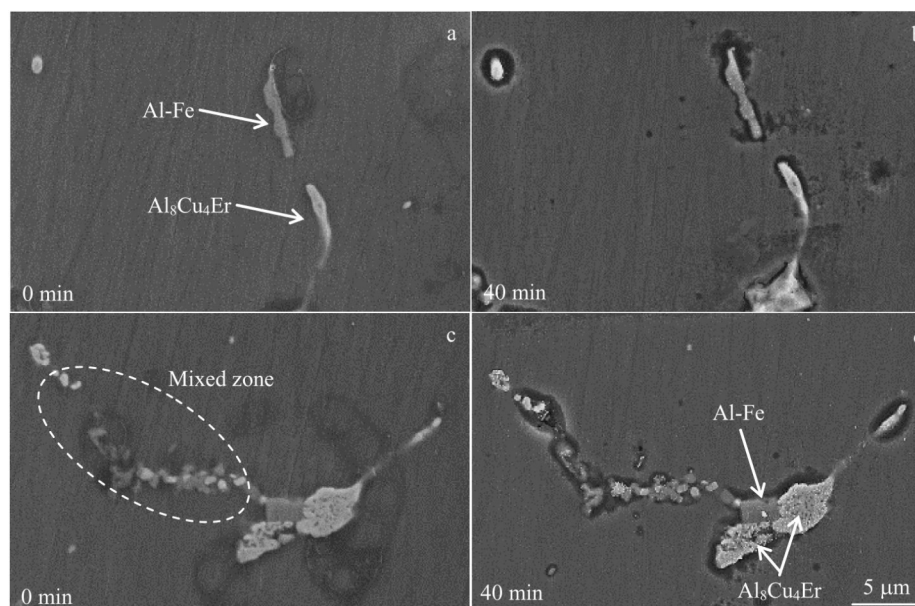


Fig.8 Spot corrosion image of alloy 3#: (a, c) no corrosion and (b, d) corrosion for 40 min

resistance of the independent Al₈Cu₄Er phase is stronger than that of the Al-Fe phase. Given the same size, the surrounding grain corrosion area is far smaller than that of the Al-Fe phase. However, the overall corrosion performances of alloy decline significantly when two phases are in the particle-bulk hybrid state.

In Cu-containing 7xxx series alloys, Cu element produces a lot of insoluble phases at crystal boundary, which generally worsens the corrosion resistance of alloys. Meanwhile, Cu interacts with Er clearly even when Cu content is low (1wt%, compared to other alloys with high Cu content), forming the Al₈Cu₄Er phase. The Al₈Cu₄Er phase possesses better resistance to pit corrosion than the Al-Fe phase, and it also may break the continuity of the secondary phase in alloys. Hence, the formation of the Al₈Cu₄Er phase and its association with the Al-Fe phase are the key to control the formation, growth and distribution of the Al₈Cu₄Er phase through composition design as well as to improve the alloying effect under the existence of rare earth elements like Er.

3 Conclusions

1) In Al-Zn-Mg-Er-Sr-Zr alloy, adding Cu can significantly hinder grain growth and decrease grain size by increasing the grain boundary secondary phases. However, the formed secondary phases are difficult to decompose during solid solution. With 0.5wt% Cu content, it is easy to form continuous networked residual phases. The secondary phases are relatively dispersed in the 1wt% Cu-contained alloy with small grain sizes.

2) There are interactions among Cu, Fe and Er. Al₆Fe can interact with Cu to form the Al₆₀Cu₃₀Fe₁₀ phase and further interact with Er to form the Al₈Cu₄Er phase. With the change of Cu and Er contents, the Al₈Cu₄Er phase grows gradually until it is separated from the associated Al-Fe phase.

3) Intergranular corrosion of alloys with different Cu contents exhibits pitting corrosion characteristics that are closely related to residual phases. With 0.5wt% Cu, Cu and Er are dissolved in the Al-Fe phase, making it form in network distribution, and the depth of pit corrosion thus increases to some extent. Compared with the Al-Fe phase, the Al₈Cu₄Er phase shows better corrosion resistance. However, coarsening of Al₈Cu₄Er phase as well as interactive relationship with the Al-Fe phase cause a sharp reduction in corrosion resistance of alloys.

References

- 1 Mikhaylovskaya A V, Kotov A D, Pozdniakov A V et al. *Journal of Alloys and Compounds*[J], 2014, 599: 139
- 2 Liao Yuguo, Han Xiaoqi, Zeng Miaoxia et al. *Materials and Design*[J], 2015, 66: 581
- 3 Sun Yuanwei, Pan Qinglin, Lin Sen et al. *Journal of Materials Research and Technology*[J], 2021, 12: 1303
- 4 Fang H C, Chao H, Chen K H et al. *Materials Science and Engineering A*[J], 2014, 610: 10
- 5 Tian Shaokun, Li Jingyuan, Zhang Junlong et al. *Journal of Materials Research and Technology*[J], 2019, 8: 4130
- 6 Gao Yan, Chen Wenlin, Guo Zhen et al. *Rare Metal Materials and Engineering*[J], 2017, 46(8): 2070
- 7 Li J H, Wiessner M, Albu M et al. *Materials Characterization*[J], 2015, 102: 62
- 8 Mandal P K. *Materials Today: Proceedings*[J], 2021, 44: 1050
- 9 Wang Yichang, Wu Xiaodong, Gao Lingfei et al. *Materials Science and Engineering A*[J], 2020, 792: 139 807
- 10 Bai Song, Liu Zhiyi, Li Yuntao et al. *Materials Science and Engineering A*[J], 2010, 527: 1806
- 11 Zhao Zhongkui, Zhou Tietiao, Liu Peiyong et al. *Rare Metal*

- Materials and Engineering*[J], 2004, 33(10): 1108 (in Chinese) Chinese)
- 12 Yang Junjun, Nie Zuoren, Jin Tounan et al. *The Chinese Journal of Nonferrous Metals*[J], 2004, 14(4): 620 (in Chinese)
- 13 Li Jinfeng, Liu Danyang, Zheng Ziqiao et al. *Acta Metallurgica Sinica*[J], 2016, 52(7): 821 (in Chinese)
- 14 Huang Yuanchun, Zhang Chuanchao, Ren Xianwei et al. *Rare Metal Materials and Engineering*[J], 2019, 48(9): 2848 (in Chinese)
- 15 Shi Weining, Zhou Haifei, Zhang Xinfang et al. *Acta Metallurgica Sinica (English Letters)*[J], 2020, 33: 1379
- 16 Dong Pengxuan, Chen Songyi, Chen Kuanghua et al. *Journal of Alloys and Compounds*[J], 2019, 788: 329
- 17 Birbilis N, Cavanaugh M K, Buchheit R G et al. *Corrosion Science*[J], 2006, 48: 4202

Cu 元素对 Al-Zn-Mg-Er-Sc-Zr 合金组织演变和腐蚀性能的影响

孟令刚¹, 武晓辉¹, 邢清源², 亚 斌¹, 周秉文¹, 朱秀荣³, 张兴国¹

(1. 大连理工大学 材料科学与工程学院, 辽宁 大连 116024)

(2. 中国航发北京航空材料研究院, 北京 100095)

(3. 中国兵器科学研究院宁波分院, 浙江 宁波 315103)

摘 要: 利用 Cu 元素的含量变化研究了 Al₈Cu₄Er 相的形成与演变规律及其对 Al-Zn-Mg-Er-Sc-Zr 合金腐蚀性能的影响。结果表明: 随着 Cu 含量的增加, 合金晶粒得到显著细化, 但同时固溶态合金不同类型的残余相增多; Al₈Cu₄Er 相与 Al-Fe 相存在伴生关系, 二者通过 Cu 与 Fe 交互作用实现相的转化, 且可表述为如下关系式: Al₆Fe $\xrightarrow{\text{Cu}}$ Al₆₀Cu₃₀Fe₁₀ $\xrightarrow{\text{Er}}$ Al₈Cu₄Er; 不同成分合金的晶间腐蚀均表现出与残余相密切相关的点蚀特征, 含 Cu、Er 的 Al-Fe 相虽然具有更小的腐蚀坑尺寸, 但网状分布特征使腐蚀深度有所增加; 而具有更好耐蚀性能的 Al₈Cu₄Er 则因相的粗化和它与 Al-Fe 相的伴生关系导致合金耐蚀性能严重下降。

关键词: Al-Zn-Mg-Cu-Er 铝合金; Al₈Cu₄Er 相; Al-Fe 相; 腐蚀性能

作者简介: 孟令刚, 男, 1983 年生, 博士, 副教授, 大连理工大学材料科学与工程学院, 辽宁 大连 116024, E-mail: menglg@dlut.edu.cn